



An Advanced Quaternary Composite for Efficient Water Splitting

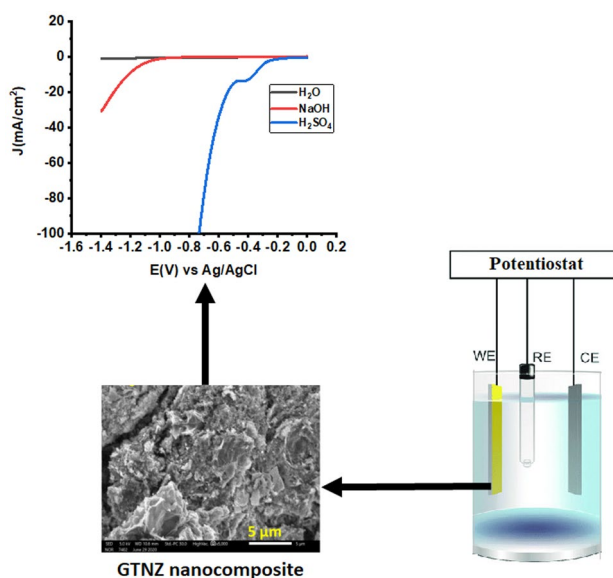
Mizaj Shabil Sha¹ · Farzana N. Musthafa¹ · Assem Alejli¹ · Johaina Khalid Alahmad¹ · Bagmita Bhattacharyya¹ · Bijandra Kumar² · Aboubakr M. Abdullah¹ · Kishor Kumar Sadasivuni¹

Received: 1 February 2023 / Accepted: 2 April 2023
© The Author(s) 2023

Abstract

Electrochemical water splitting is a promising pathway for effective hydrogen (H_2) evolution in energy conversion and storage, with electrocatalysis playing a key role. Developing efficient, cost-effective and stable catalysts or electrocatalysts is critical for hydrogen evolution from water splitting. Herein, we evaluated a graphene-modified nanoparticle catalyst for hydrogen evolution reaction (HER). The electrocatalytic H_2 production rate of reduced graphene oxide-titanium oxide-nickel oxide-zinc oxide (rGO-TiO₂-NiO-ZnO) is high and exceeds that obtained on components alone. This improvement is due to the presence of rGO as an electron collector and transporter. Moreover, a current density of 10 mA/cm² was recorded at a reduced working potential of 365 mV for the nanocomposite. The electronic coupling effect between the nanoparticle components at the interface causes the nanoparticle's hydrogen evolution reaction catalytic activity.

Graphical Abstract



Keywords Electrochemical hydrogenation · Graphene oxide · Titanium oxide · Electrocatalysts

✉ Kishor Kumar Sadasivuni
kishor_kumars@yahoo.com

¹ Center for Advanced Materials, Qatar University, P. O. Box 2713, Doha, Qatar

² Department of Technology, Elizabeth City State University, Elizabeth City, USA

1 Introduction

Global environmental degradation and reducing non-renewable energy resources enhance the need for renewable energy sources. Hydrogen is one such source that can replace fossil fuels [1]. Electrochemical water splitting has received

immense attention among the various hydrogen production methods because of its high efficiency, mild conditions, low energy input, and ease of manipulation [2, 3]. An electrochemical cell with water as an electrolyzer can produce hydrogen [4]. Noble metals, or platinum group materials, are currently the most efficient electrocatalysts for HER, but their scarcity and high cost make them unsuitable for large-scale applications [5–7]. Exploring cost-effective alternatives to platinum group catalysts is critical for making HER more widely available [8].

Over the last few decades, several semiconductors have been investigated as anodes for HER. Earth-abundant metal oxides have generated the most intense interest in intermediate bandgaps [9–11]. However, charge recombination, poor electrical conductivity, and slow oxygen evolution reaction (OER) kinetics impede anode performance. Various techniques, including doping, morphology engineering, and surface modification, have been investigated to address these limitations [12, 13].

These techniques provide a viable method for promoting charge carrier mobility between different components, thereby improving composite separation and photoactivity [14, 15]. Significantly improved performance has been achieved by incorporating metal oxides [16–18]. Nonetheless, the most difficult problem is identifying more efficient metal oxide-based heterojunctions [19].

Nanoparticles were fabricated and used to build metal oxide heterostructured anodes in this paper. Because of the improved charge separation and strong interfacial interaction, the rGO-TiO₂-NiO-ZnO (GTNZ) composite demonstrated improved electrochemical activity [20–22]. Reduced graphene oxide (rGO) acts as a passivation layer, preventing corrosion and improving catalyst performance [23]. On the other hand, titanium dioxide (TiO₂) is regarded as the standard gold semiconductor in electrocatalysis because it has a suitable band structure and allows the overall water-splitting reaction to occur thermodynamically [24]. NiO acts as a water oxidation cocatalyst, suppressing the recombination of induced electron and hole pairs, resulting in increased catalytic activity in the system [25]. ZnO generally has n-type conductivity, and the difficulty in preparing p-type to form stable p-n junctions limits its commercial application [26, 27]. The nanocomposite demonstrated a superior current density of 10 mA/cm² at a reduced working potential of 365 mV vs RHE. This heterostructured anode's open circuit potential is higher than that of pristine metal oxides and superior to several other metal oxide-based photoanodes. The high and consistent response over 24 h confirms the heterostructure's good stability for hydrogen production.

2 Methodology

2.1 Chemicals Used

Zinc nitrate (98%), graphite (99% carbon basis), sodium borohydride (powder, ≥ 98.0%) and nickel nitrate (crystallized, 99.9%) were purchased from SRL. Sodium hydroxide (≥ 98.0%), nafion (~ 5% in a mixture of lower aliphatic alcohols and water), ethanol (95%), titanium isopropoxide (97%), acetyl trimethylammonium bromide (99%), and glacial acetic acid (99%) and sulphuric acid (985–98%) were purchased from Rankem, India.

2.2 Nanoparticles and Electrodes Preparation

The modified Hummer method produced graphene oxide (GO) by oxidizing graphite [28]. The quaternary composite was prepared using the sol-gel process. Titanium isopropoxide was hydrolyzed in the first step using glacial acetic acid (1–2) at 30 °C by adding 80 mL of ethanol. To achieve complete homogeneity, the mixture was stirred for 20 min. In 80 mL of deionized water, Ni(NO₃)₂ (0.1 wt%) and Zn(NO₃)₂ (0.1 wt%) were ultrasonically dispersed. To deposit nickel oxide-zinc oxide (NiO-ZnO) onto the surface of TiO₂ nanoparticles, 2 mL of 0.5 M Sodium borohydride (NaBH₄) solution was added to the TiO₂ nanoparticle suspension while continuously stirring at 30 °C. Continuous stirring at 50 °C for 10 h completed the TiO₂-NiO-ZnO reaction. Graphene oxide (GO) suspension (40 mg) and acetyl trimethylammonium bromide (CTAB, 1 g) were mixed in 60 mL of ethanol for half an hour before placing in a 250 mL beaker and dropwise added into the above TiO₂-NiO-ZnO solution. After complete hydrolysis, a gelly mixture was formed. The product was dried in an 80 °C vacuum oven overnight. The gel material was then calcined in air for 5 min at 500 °C to produce a mixed oxide nanocomposite. The same method was used to create rGO-TiO₂, rGO-TiO₂-NiO, and rGO-TiO₂-ZnO nanocomposites, as described above.

A homogeneous catalytic ink was prepared to make electrodes by ultrasonically mixing 20 mg of nanopowder, 2 mL of ethanol, and 20 μL of Nafion solution. The working electrode was cleaned with distilled water and polished with aluminium oxide powder. Then, 10 μL of catalytic ink was uniformly coated on the surface of glassy carbon electrodes (GCE) and dried at ambient conditions.

2.3 Characterization of Nanoparticle

The crystal phases were collected using an X-ray diffractometer (XRD-6100, LabX, SHIMADZU Ltd., Japan). A Thermo Nicolet Nexus 670 FTIR spectrometer (KBr pellets)

was used to investigate and confirm the molecular structure. The surface structure of the nano-catalysts was examined using a scanning electron microscope (SEM) (Hitachi S-4800, Japan).

2.4 Electrochemical Characterization

The electrochemical analysis was carried out on a three-electrode gamry potentiostat. Graphite and Ag/AgCl electrodes were used as the counter and reference electrodes. The glassy carbon was coated with the prepared nanopowder. All electrochemical measurements were carried out in electrolytes containing 0.5 M H₂SO₄. To obtain the polarization curves, linear sweep voltammetry (LSV) experiments were carried out from 0–1.4 V (vs RHE) at a sweep rate of 0.5 mV s⁻¹.

3 Results and Discussions

3.1 physical Characterizations

Figure 1 depicts the XRD pattern of rGO, TiO₂, NiO, ZnO and GTNZ nanocomposites. The TiO₂ nanoparticles were represented by major XRD peaks at 2θ of 25.4°, 48°, 55.2°, and 62.8° [29]. Diffraction peaks revealed the formation of crystalline NiO onto the GTNZ at 2θ values of 37.1°, 62.8°, and 75.4°, and peaks revealed peaks of ZnO at 31.8°, 34°, 36.9°, 47.7°, 56.7°, 62.95°, and 68° correspond to crystal planes of the hexagonal. [30] Few peaks on the rGO surface indicated that the carbonaceous surface was well-exfoliated and covered by other metal oxides. GTNZ diffraction peaks were sharper, indicating better crystallinity.

The FTIR spectra of individual nanoparticles and the composite are shown in Fig. 1b. The highest band at 3550–3350 cm⁻¹ is typical of OH stretching and is primarily attributed to surface-adsorbed water. Several bands can be seen in the 1750–850 cm⁻¹ range. Ti–O and

Ti–O–Ti stretching vibration modes are assigned peaks at 1450–1400 cm⁻¹ and below 850 cm⁻¹. Metal–oxygen (Zn–O, Ni–O) peaks are detected at 443 cm⁻¹. At around 1386 cm⁻¹, a bending vibration peak can be seen as adsorbed water molecules. NO₃⁻'s characteristic vibration causes a distinct absorption peak at 1612 cm⁻¹. The absorption peak at 2348 cm⁻¹ is caused by oxygen–oxygen bonds (O–O). Furthermore, a broad peak appears at a high wave number of 3450 cm⁻¹, representing the stretching vibration of O–H. The absorption band is caused by water generated by metal hydroxyl group bonds and hydrogen bonds [31, 32].

The SEM images in Fig. 2 show GO with a smooth surface and numerous folds, but they became rougher after TiO₂, NiO and ZnO nanoparticles were anchored on rGO layers. Furthermore, the presence of TiO₂, NiO and ZnO nanoparticles on rGO decreased the number of folds and increased the interlayer distance between the layers.

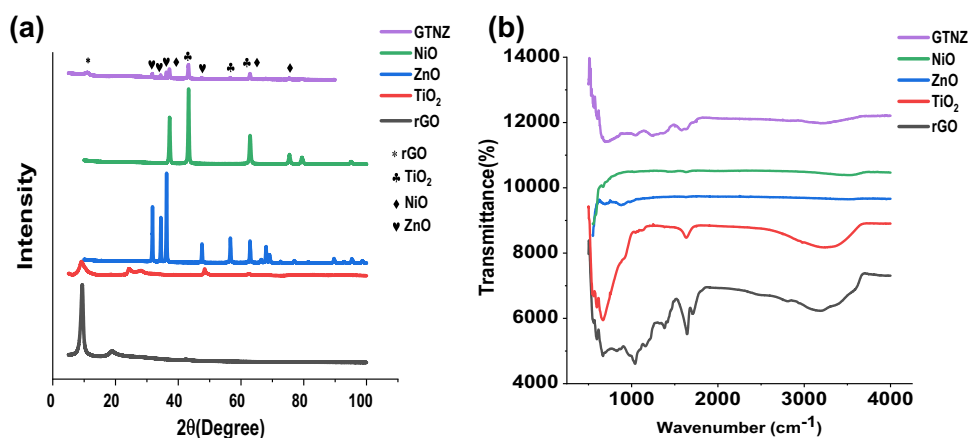
Figure 3f represents the EDS spectra of elements in the composite. The marked peaks represent the elements, and the remaining peaks represent impurities.

3.2 Electrochemical Performance

Figure 3a depicts the HER activity of GTNZ on GCE measured using LSV at a scan rate of 5 mV s⁻¹ in 1 M NaOH, 0.5 M H₂SO₄ and DI water. Due to its insignificant participation in HER activity, GCE was chosen for HER. The study discovered that HER evaluation in 0.5 M H₂SO₄ produced better results than basic and neutral electrolytes. The GTNZ NPs have an HER onset potential of 365 mV vs RHE, which is accompanied by visual detection of the formation of H₂-gas bubbles near the electrode surface. For further investigation, 0.5 M H₂SO₄ was used as it produced more hydrogen compared to other electrolytes.

The HER performance of the quaternary composite components was also evaluated (Fig. 3b and c). The quaternary composite was observed to have low over potential compared to individual components and other possible

Fig. 1 a XRD pattern b FTIR spectra



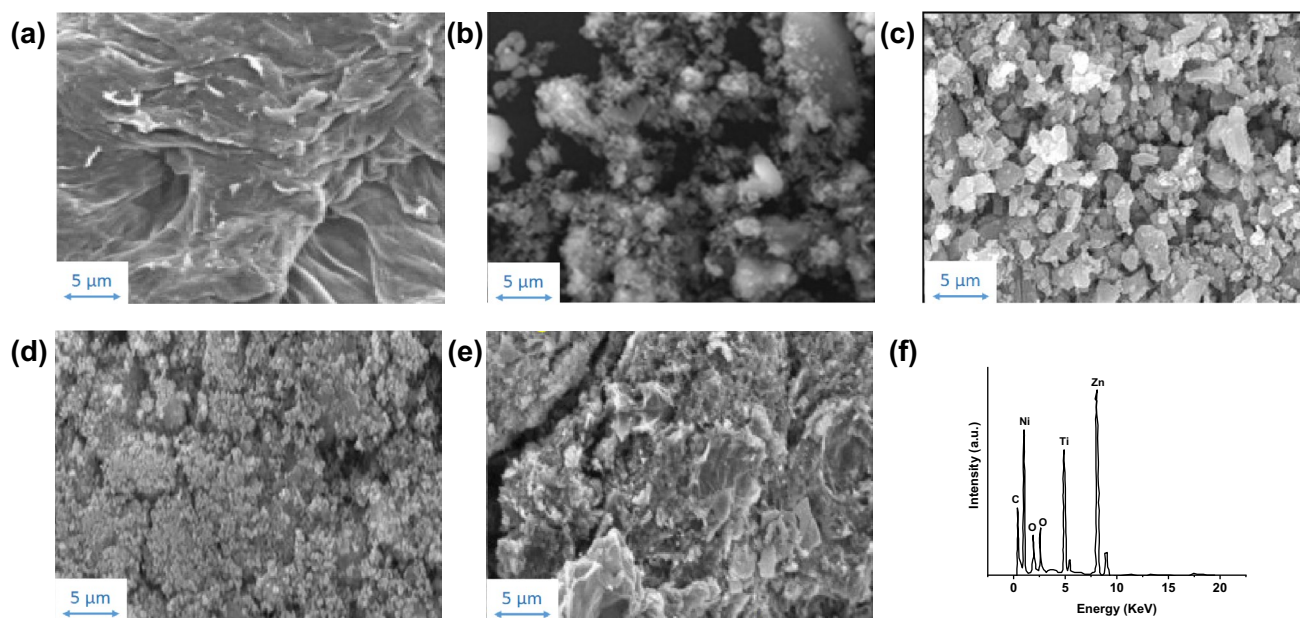


Fig. 2 SEM images of **a** GO, **b** TiO₂, **c** NiO, **d** ZnO and **e** GTNZ, **f** Elemental mapping of components

Fig. 3 HER performance **a** different electrolytes, **b** Individual components, **c** nanocomposites **d** comparison with Pt/C electrode

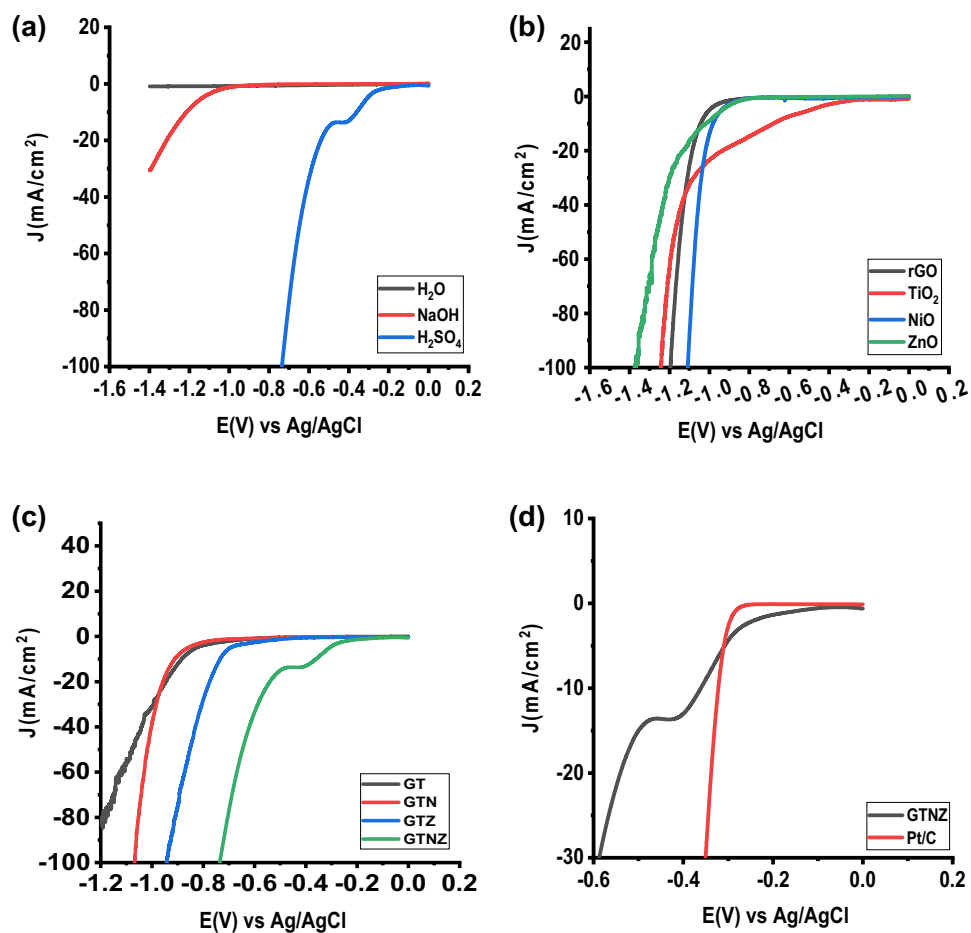


Table 1 HER performance of components and composites

| Sl. No | The catalyst used for HER activity in 0.5 M H ₂ SO ₄ solution | η (Over potential in mV) | Tafel Slope (mV/dec) |
|--------|---|-------------------------------|----------------------|
| 1 | rGO | 1040 | 118 |
| 2 | TiO ₂ | 689 | 89 |
| 3 | NiO | 986 | 73 |
| 4 | ZnO | 1038 | 96 |
| 5 | GT | 884 | 130 |
| 6 | GTN | 926 | 102 |
| 7 | GTZ | 739 | 136 |
| 8 | GTNZ | 365 | 56 |

composites (Table 1). Other components require significantly higher HER overpotentials to achieve 10 mA cm⁻², indicating that the GTNZ NPs have distinct HER catalytic activity. For a current density of 10 mA cm⁻², GTNZ NP has the lowest 365 mV compared to other catalysts. In acid media, this HER performance is comparable to the benchmark Pt catalyst (20% Pt/C) supported on GCE at the same catalyst loading (Fig. 3d).

The catalyst's stability was also tested under fixed current conditions (Fig. 4a). The stability test was set up using chronoamperometry at 365 mV for $j_{\text{HER}} = 10 \text{ mA cm}^{-2}$. GTNZ is found to be stable for an extended period of 4 h at a constant current (10 mA cm⁻²). During the first hour of electrolysis, no metal dissolution was observed. A trace amount of GTNZ was detected in the electrolyte after 4 h of electrolysis, corresponding to only 2 wt% GTNZ in the fresh electrode.

To investigate the HER reaction kinetics, Tafel plots were generated from the LSVs, as shown in Fig. 4b. The GTNZ has a much lower slope of 56 mV dec⁻¹ in acidic media than rGO NP (118 mV dec⁻¹), TiO₂ NP (89 mV dec⁻¹), NiO NP (73 mV dec⁻¹), and ZnO NP (96 mV dec⁻¹). This slope value also differs significantly from previously reported

GT-based catalysts, which typically exhibit Tafel slopes greater than 80 mV dec⁻¹ and approaches Pt/C electrodes (Tafel slope: 50 mV dec⁻¹), implying that the HER at the GTNZ NP is a Volmer-Heyrovsky HER mechanism.

Furthermore, GTNZ was used as both the anode and cathode in a whole-cell water electrolyzer. The GTNZ cell's polarization curve is recorded. The GTNZ NP cell was monitored for stability for 24 h, as shown in Fig. 5a. Throughout the experiment, the cell was extremely stable. We also looked at how the temperature of the environment affected HER performance. The experiment was conducted at five different temperatures: 35, 45, 55, 65, and 75 °C. The best results were obtained at room temperature. There was no correlation found for elevated temperatures (Fig. 5b).

Electrochemical impedance spectroscopy (EIS) data were collected at 1.23 Vs. Ag/AgCl in the sweeping frequency of 0.1 Hz–100 kHz. The blank electrode had an Rct ~ 700, while the GTNZ electrode had 470. The linear part (diffusion impedance) of the GTNZ electrode was less than that of the blank electrode combinations at lower frequencies, indicating that the diffusion process was taking place with much lower resistance, thereby improving mass transportation (ions from the bulk to the electrode surface). It confirms that the GTNZ electrodes have more electron conduction pathways and reactive surfaces, which results in better electrolyte diffusion on the electrode surface (Fig. 6a).

Figure 6b represents the SEM image of GTNZ after hydrogen evolution reaction. Furthermore, it was observed that as a result of hydrogen evolution reaction, the number of folds were decreased and increased the interlayer distance between the layers compared to Fig. 2e.

4 Conclusion

In conclusion, this study shows that using GTNZ as an electrocatalyst can produce previously unseen synergistic effects in electrocatalysis. This method overcomes the

Fig. 4 a stability analysis b Tafel plots for all nanoparticles

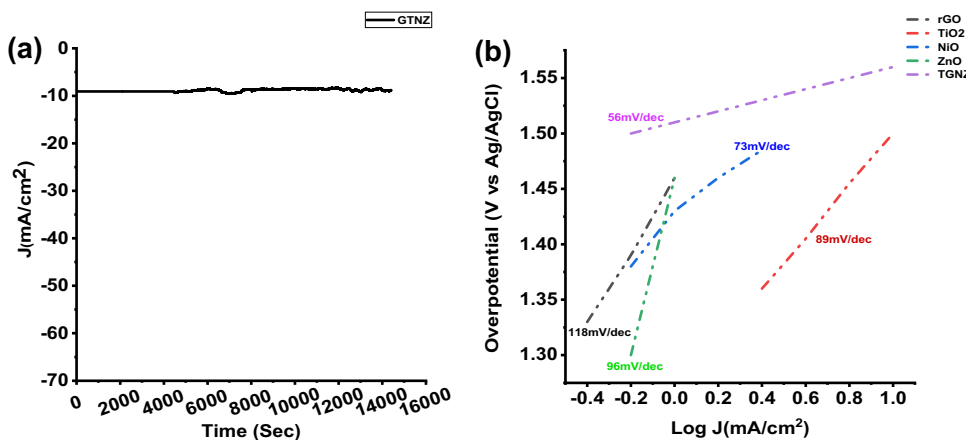


Fig. 5 **a** stability analysis of GTNZ/GTNZ electrodes **b** effect of temperature

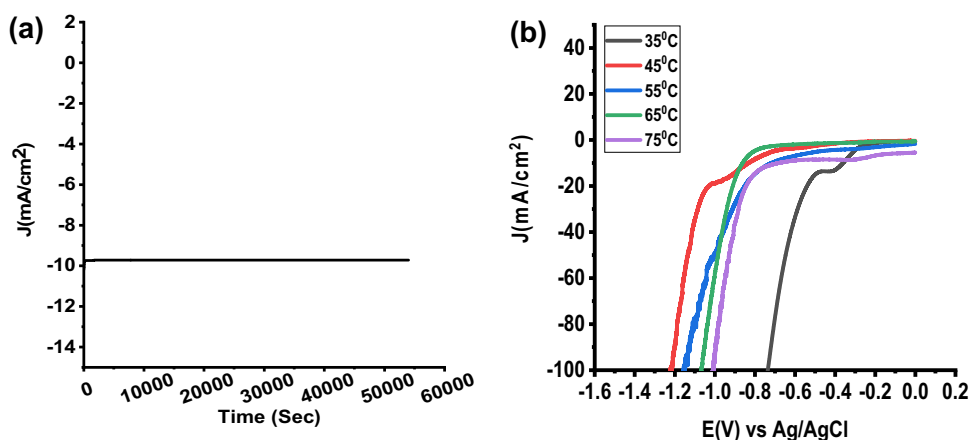
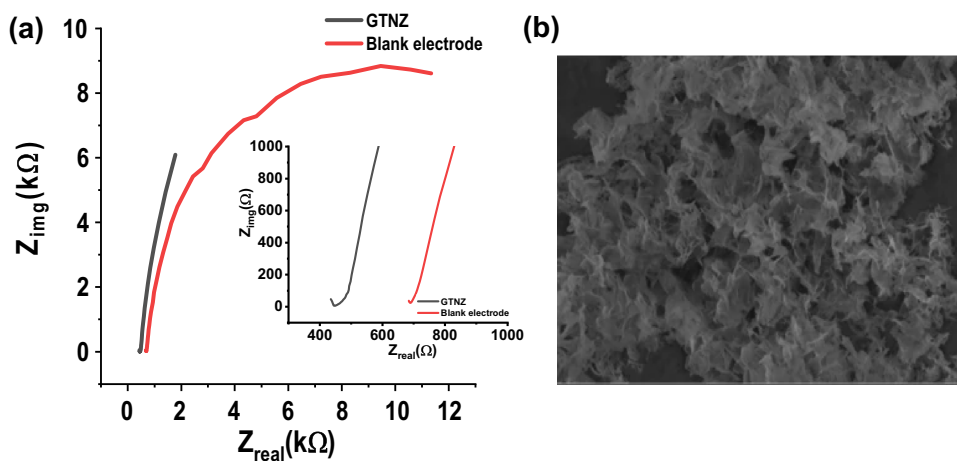


Fig. 6 **a** EIS spectra of GTNZ and blank electrodes. **b** SEM image of GTNZ after HER



practical limitation of low HER activity on mixed oxides for overall water electrolysis. Furthermore, this electrocatalyst is highly capable of preserving catalyst structure and activity during power outages, making it ideal for a water electrolyzer powered by intermittent renewable energy sources. We hope this catalyst design will aid in developing other multimetallic nanoparticle electrocatalysts with varying compositions and structures and distinct interfaces for use in various electrolytic applications such as carbon dioxide reduction reactions and nitrogen reduction reactions.

Acknowledgement This work was supported by the Qatar National Research Fund (a member of Qatar Foundation) grants NPRP11S-1221-170116. The statements made herein are solely the responsibility of the authors.

Funding Open Access funding provided by the Qatar National Library.

Declarations

Conflict of interest The authors declare that they have no conflict of interest.

Open Access This article is licensed under a Creative Commons Attribution 4.0 International License, which permits use, sharing, adaptation, distribution and reproduction in any medium or format, as long as you give appropriate credit to the original author(s) and the source, provide a link to the Creative Commons licence, and indicate if changes were made. The images or other third party material in this article are included in the article's Creative Commons licence, unless indicated otherwise in a credit line to the material. If material is not included in the article's Creative Commons licence and your intended use is not permitted by statutory regulation or exceeds the permitted use, you will need to obtain permission directly from the copyright holder. To view a copy of this licence, visit <http://creativecommons.org/licenses/by/4.0/>.

References

- Al-Shetwi AQ (2022) Sustainable development of renewable energy integrated power sector: trends, environmental impacts, and recent challenges. *Sci Total Environ* 822:153645. <https://doi.org/10.1016/j.scitotenv.2022.153645>
- Suryanto BHR, Wang Y, Hocking RK et al (2019) Overall electrochemical splitting of water at the heterogeneous interface of nickel and iron oxide. *Nat Commun* 10:5599. <https://doi.org/10.1038/s41467-019-13415-8>
- Kamaroddin MFA, Sabli N, Abdullah TAT et al (2021) Membrane-based electrolysis for hydrogen production: a review. *Membranes*. <https://doi.org/10.3390/membranes11110810>
- Qazi UY (2022) Future of hydrogen as an alternative fuel for next-generation industrial applications. *Chall Expect Oppor Energ* 15:4741. <https://doi.org/10.3390/en15134741>
- Serov A, Kovnir K, Shatruk M, Kolen'ko YV, (2021) Critical review of platinum group metal-free materials for water electrolysis: transition from the laboratory to the market. *Johns Matthey Technol Rev* 65:207–226. <https://doi.org/10.1595/205651321X16067419458185>
- Costa de Oliveira MA, D'Epifanio A, Ohnuki H, Mecheri B (2020) Platinum group metal-free catalysts for oxygen reduction reaction: applications in microbial fuel cells. *Catalysts* 10:475. <https://doi.org/10.3390/catal10050475>
- Kumar S, Kaur R, Sharma S (2022) Recent reports on hydrogen evolution reactions and catalysis. *Results Chem* 4:100613. <https://doi.org/10.1016/j.rechem.2022.100613>
- Abbas M, Bang JH (2015) Rising again: opportunities and challenges for platinum-free electrocatalysts. *Chem Mater*. <https://doi.org/10.1021/acs.chemmater.5b03331>
- Avcioglu C, Avcioglu S, Bekheet MF, Gurlo A (2022) Solar hydrogen generation using niobium-based photocatalysts: design strategies, progress, and challenges. *Mater Today Energy* 24:100936. <https://doi.org/10.1016/j.mtener.2021.100936>
- Augustynski J, Alexander B, Solarz R (2011) Metal oxide photoanodes for water splitting. *Top Curr Chem* 303:1–38. https://doi.org/10.1007/128_2011_135
- Eidsvåg H, Bentouba S, Vajeeston P et al (2021) TiO₂ as a photocatalyst for water splitting—an experimental and theoretical review. *Molecules* 26:1687. <https://doi.org/10.3390/molecules26061687>
- Aguilera González EN, Estrada-Flores S, Martínez-Luévanos A (2021) Nanomaterials: Recent Advances for Hydrogen Production. In: Kharissova OV, Torres-Martínez LM, Kharisov BI (eds) *Handbook of nanomaterials and nanocomposites for energy and environmental applications*. Springer International Publishing, Cham, pp 2767–2792
- Mikaeili F, Gilmore T, Gouma P-I (2022) Photochemical water splitting via transition metal oxides. *Catalysts* 12:1303. <https://doi.org/10.3390/catal12111303>
- Ye X, Zhu T, Hui Z et al (2021) Revealing the transfer mechanisms of photogenerated charge carriers over g-C₃N₄/ZnIn₂S₄ composite: a model study for photocatalytic oxidation of aromatic alcohols with visible light. *J Catal* 401:149–159. <https://doi.org/10.1016/j.jcat.2021.07.025>
- R. Fareza A, Ardy Nugroho FA, F. Abdi F, Fauzia V, (2022) Nanoscale metal oxides–2D materials heterostructures for photoelectrochemical water splitting—a review. *J Mater Chem A* 10:8656–8686. <https://doi.org/10.1039/D1TA10203F>
- Bhanja P, Kim Y, Paul B et al (2020) Facile synthesis of nanoporous transition metal-based phosphates for oxygen evolution reaction. *ChemCatChem* 12:2091–2096. <https://doi.org/10.1002/cctc.201901803>
- Guo Y, Zhang C, Zhang J et al (2021) Metal-organic framework-derived bimetallic NiFe selenide electrocatalysts with multiple phases for efficient oxygen evolution reaction. *ACS Sustainable Chem Eng* 9:2047–2056. <https://doi.org/10.1021/acssuschemeng.0c06969>
- Ao K, Wei Q, Daoud WA (2020) MOF-derived sulfide-based electrocatalyst and scaffold for boosted hydrogen production. *ACS Appl Mater Interfaces* 12:33595–33602. <https://doi.org/10.1021/acami.0c04302>
- Anucha CB, Altin I, Bacaksiz E, Stathopoulos VN (2022) Titanium dioxide (TiO₂)-based photocatalyst materials activity enhancement for contaminants of emerging concern (CECs) degradation: in the light of modification strategies. *Chem Eng J Adv* 10:100262. <https://doi.org/10.1016/j.cej.2022.100262>
- Guo Y, Zhou X, Tang J et al (2020) Multiscale structural optimization: highly efficient hollow iron-doped metal sulfide heterostructures as bifunctional electrocatalysts for water splitting. *Nano Energy* 75:104913. <https://doi.org/10.1016/j.nanoen.2020.104913>
- Hu S, Wang S, Feng C et al (2020) Novel MOF-derived nickel nitride as high-performance bifunctional electrocatalysts for hydrogen evolution and urea oxidation. *ACS Sustain Chem Eng* 8:7414–7422. <https://doi.org/10.1021/acssuschemeng.0c01450>
- Septiani NLW, Kaneti YV, Fathoni KB et al (2020) Tailorable nano-architecture of bimetallic nickel–cobalt hydrogen phosphate via the self-weaving of nanotubes for efficient oxygen evolution. *J Mater Chem A* 8:3035–3047. <https://doi.org/10.1039/C9TA13442E>
- Luo X, Zhong J, Zhou Q et al (2018) Cationic reduced graphene oxide as self-aligned nanofiller in the epoxy nanocomposite coating with excellent anticorrosive performance and its high antibacterial activity. *ACS Appl Mater Interfaces* 10:18400–18415. <https://doi.org/10.1021/acsami.8b01982>
- Le Bahers T, Takanabe K (2019) Combined theoretical and experimental characterizations of semiconductors for photo electrocatalytic applications. *J Photochem Photobiol C* 40:212–233. <https://doi.org/10.1016/j.jphotochemrev.2019.01.001>
- Fo Y, Wang M, Ma Y et al (2020) Origin of highly efficient photocatalyst NiO/SrTiO₃ for overall water splitting: insights from density functional theory calculations. *J Solid State Chem* 292:121683. <https://doi.org/10.1016/j.jssc.2020.121683>
- Jian J, Kumar R, Sun J (2020) Cu₂O/ZnO p–n junction decorated with NiOx as a protective layer and cocatalyst for enhanced photoelectrochemical water splitting. *ACS Appl Energy Mater* 3:10408–10414. <https://doi.org/10.1021/acsaem.0c01198>
- Isaev AB, Shabanov NS, Sobola D et al (2022) ZnO/Chalcogenides semiconductor heterostructures for photoelectrochemical water splitting. In: Kasinathan K, Elshikh MS, Al Farraj DA-A (eds) *Nanomaterials for energy conversion, biomedical and environmental applications*. Springer Nature, Singapore, pp 3–35
- Kaur M, Kaur H, Kukkar D (2018) Synthesis and characterization of graphene oxide using modified Hummer's method. *AIP Conf Proc* 1953:030180. <https://doi.org/10.1063/1.5032515>
- Santhosh K, Sk S, Chouti S et al (2021) Tailoring hierarchical porous TiO₂ based ternary rGO/NiO/TiO₂ photocatalyst for efficient hydrogen production and degradation of Rhodamine B. *J Mol Struct* 1235:130222. <https://doi.org/10.1016/j.molstruc.2021.130222>
- Chen Z, Gao Y, Zhang Q et al (2019) TiO₂/NiO/reduced graphene oxide nanocomposites as anode materials for high-performance lithium-ion batteries. *J Alloy Compd* 774:873–878. <https://doi.org/10.1016/j.jallcom.2018.10.010>
- Leal JF, Cruz SMA, Almeida BTA et al (2020) TiO₂–rGO nanocomposite as an efficient catalyst to photodegrade formalin in aquaculture waters, under solar light. *Environ Sci* 6:1018–1027. <https://doi.org/10.1039/C9EW00950G>
- Zheng J, Zhang R, Wang X, Yu P (2018) Synthesizing a flower-like NiO and ZnO composite for supercapacitor applications. *Res Chem Intermed*. <https://doi.org/10.1007/s11164-018-3441-x>